

Collateral Coupling between Superconducting Resonators: Fast High-Fidelity Generation of Qudit-Qudit Entanglement

Pedro Rosario^{1,*}, Alan C. Santos^{1,†}, C.J. Villas-Boas^{1,‡} and R. Bachelard^{1,2,§}

¹Departamento de Física, Universidade Federal de São Carlos, Rodovia Washington Luís, km 235 - SP-310, São Carlos, SP 13565-905, Brazil

²Université Côte d'Azur, CNRS, Institut de Physique de Nice, Valbonne 06560, France

(Received 5 May 2023; revised 5 July 2023; accepted 28 August 2023; published 15 September 2023)

Superconducting circuits are highly controllable platforms to manipulate quantum states, which make them particularly promising for quantum information processing. We show here how the existence of a distance-independent interaction between microwave resonators coupled capacitively through a qubit offers an alternative control parameter toward this goal. This interaction is able to induce an idling point between resonant resonators, and its state-dependent nature allows one to control the flow of information between the resonators. The advantage of this scheme over the previous one is demonstrated through the generation of high-fidelity NOON states between the resonators, with a lower number of operations than previous schemes. Beyond superconducting circuits, our proposal could also apply to atomic lattices with clock transitions in optical cavities, for example.

DOI: 10.1103/PhysRevApplied.20.034036

I. INTRODUCTION

Superconducting integrated circuits [1–4] are currently one of the most promising platforms for building quantum computers, due to their potential for scalability, multi-qubit tunable interaction, and high-fidelity processing of quantum information [5–7]. Differently from cold atoms or trapped ions, the coupling between the components of a circuit occurs between nearest neighbors, although the physical proximity between the different components can result in additional (parasitic) couplings, generating crosstalks and affecting the fidelity of protocols [8,9]. The advantage of nearest-neighbor interactions is that a local transfer of information can be operated, while the rest of the circuit remains unaffected, using, for example, a suitable detuning between the qubits or local oscillating fields [10–15].

Of particular interest are systems of superconducting resonators, due to their high performance to mediate interaction between several qubits in integrated quantum circuits [16–20]. Furthermore, when using superconducting qubit-resonator hybrid systems to process quantum information, computation beyond qubits can be performed, where arbitrary quantum states of *qudits* can be generated [21–26]. The configuration of two resonators coupled

through an intermediate qubit has proven especially successful, with theoretical and experimental works demonstrating the generation of entangled photon Fock states [27,28], two-mode cat states of electromagnetic fields [29], and for the improvement of quantum nondemolition measurements in the Fock basis in a resonator [30].

We here discuss how the mere fact of using a qubit to transfer information from one resonator to the other actually induces a coupling between the resonators, hereafter called “collateral” coupling. Different from a mediated interaction, which is obtained from tracing over the variables of the mediating component (here the qubit), it stems from switching from the Lagrangian description of the integrated circuit, where only nearest-neighbor coupling terms are present, to its Hamiltonian representation [31,32]. Interaction of this nature also is present in the system of tunable coupling between superconducting artificial atoms [33], and for systems of atoms in optical cavities, as we shall see. In the resonator-qubit-resonator sketched in Fig. 1, a distance-independent interaction between the two resonators emerges, which scales as the product of the two direct capacitive resonator-qubit couplings.

Although the collateral term is a correction to the overall Hamiltonian, it represents a substantial contribution in the case of superconducting qubits, able to generate an idling point for the resonators dynamics. The dependence of the idling point on the qubit state provides an alternative control parameter to engineer quantum states, of which we take advantage to generate efficiently NOON states between the resonators. Finally, we discuss how the

*pedrorosario@estudante.ufscar.br

†ac_santos@df.ufscar.br

‡celsov@df.ufscar.br

§romain@ufscar.br

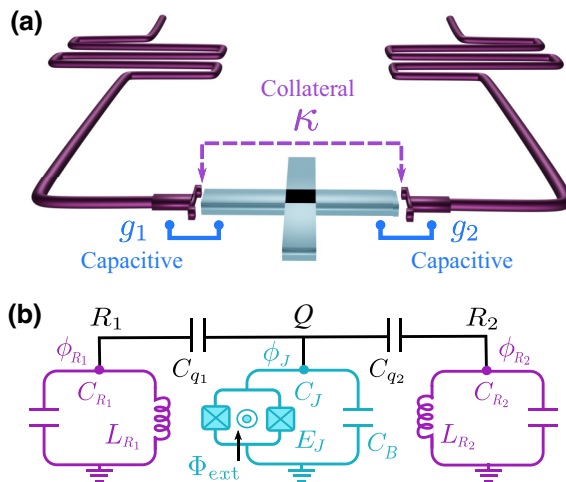


FIG. 1. (a) Two superconducting resonators (R_1, R_2) coupled to a transmon (Q) present a qubit-mediated interaction (κ) due to the capacitance network of the system and direct atom-resonator capacitive couplings (g_k). The setup is equivalent to an atom inside two crossed optical cavities. (b) Lumped superconducting circuit showing the capacitance and inductance networks.

collateral coupling term could become equally useful for other platforms, such as cold atoms with clock transitions in crossed optical cavities. As immediate applications of the theory discussed in this work, collateral interaction constitutes a timely ingredient to engineer different ranges of tunability for coupler-mediated interaction, or suppress undesired crosstalk interactions in integrated multiqubit superconducting processors [34–36].

II. MODELING OF THE SUPERCONDUCTING CIRCUIT

Let us consider a linear circuit composed of two resonators R_1 and R_2 each coupled to an intermediate qubit Q (qubit-resonator capacitance $C_{q1,2}$), see Fig. 1(b). There is no direct interaction between the resonators, a situation encountered when the distance between them is large enough to prevent parasitic coupling. The qubit is a frequency-tunable transmon [37,38], whose frequency $\omega(\Phi_{ext})$ can be tuned through the external flux Φ_{ext} , being its natural frequency $\omega_0 = \omega(\Phi_{ext} = 0)$. We assume a transmon composed of a superconducting loop with two identical Josephson junctions with energy E_J and capacitance C_J , shunted by an external capacitor C_B . As for the two resonators, they are characterized by their internal capacitance C_{Rn} and inductance L_{Rn} , with $n = 1, 2$.

The equations of motion are derived by first writing down the system Lagrangian. Applying Kirchhoff's laws and the method of nodes [32,39] to the circuit diagram presented in Fig. 1(b), we obtain the following Lagrangian

(see Appendix A for details on the derivation):

$$L(\vec{\phi}, \dot{\vec{\phi}}) = (C_T + C_{q1} + C_{q2}) \frac{\dot{\phi}_J^2}{2} + \sum_{n=1}^2 (C_{Rn} + C_{qn}) \frac{\dot{\phi}_{Rn}^2}{2} - C_{q1} \dot{\phi}_J \dot{\phi}_{R1} - C_{q2} \dot{\phi}_J \dot{\phi}_{R2} - U(\vec{\phi}), \quad (1)$$

where $\vec{\phi} = (\phi_J, \phi_{R1}, \phi_{R2})$, with ϕ_J and ϕ_{Rn} the node flux of the qubit and of the n th resonator, respectively, while $C_T = C_J + C_B$ is the total qubit box capacitance. The potential term $U(\vec{\phi})$ is given by $U(\vec{\phi}) = \phi_{R1}^2/2L_{R1} + \phi_{R2}^2/2L_{R2} - \tilde{E}_J \cos(\phi_J/\Phi_0)$, with $\tilde{E}_J = 2E_J |\cos(\pi\Phi_{ext}/\Phi_0)|$ the Josephson energy [40], and $\Phi_0 = \hbar/2e$ the quantum of magnetic flux through the qubit. Switching to the Hamiltonian formalism leads to

$$H \approx \frac{q_J^2}{2C_T} - \tilde{E}_J \cos\left(\frac{\phi_J}{\Phi_0}\right) + \frac{q_{R1}^2}{2C_{R1}} + \frac{\phi_{R1}^2}{2L_{R1}} + \frac{q_{R2}^2}{2C_{R2}} + \frac{\phi_{R2}^2}{2L_{R2}} + \frac{C_{q1}}{C_{R1}C_T} q_J q_{R1} + \frac{C_{q2}}{C_{R2}C_T} q_J q_{R2} + \frac{C_{q1}C_{q2}}{C_{R1}C_{R2}C_T} q_{R1}q_{R2}, \quad (2)$$

where we have introduced the momentum $q_k = \partial L(\vec{\phi}, \dot{\vec{\phi}})/\partial \dot{\phi}_k$, conjugate to the node flux ϕ_k . Hamiltonian (2) has been derived in the regime where $C_T = C_J + C_B \gg C_{qk}$ and $C_{Rk} \gg C_{qk}$, where corrections of the order $\mathcal{O}(C_{qk}/C_T)$ and $\mathcal{O}(C_{qk}/C_{Rk})$ are neglected.

The last term in Eq. (2) is of particular interest, since it corresponds to a direct coupling between the resonators, due to the presence of a qubit coupled to each of them. We call it “collateral” capacitive coupling: it does not correspond to a “mediated” or “effective” interaction, since we did not trace out over the qubit degree of freedom, neither did we operate a specific transformation or operation on the variables of the Hamiltonian that would make it appear (the approximation on the capacities is a mere convenience, and does not affect the existence of the collateral term). Furthermore, it cannot be considered as a parasitic coupling, which refers to an additional coupling typically due to the physical proximity of the different components [41]. Indeed, the collateral term does not depend on the distance between the resonators, but only to the capacitive coupling of each with the qubit, such that it is the dominant interaction in the limit in which parasitic couplings vanish (see Appendix A). As we discuss later, it is in essence similar to a mode-mode coupling term already derived by Fermi in the context of a charged particle interacting with electromagnetic modes [42].

We then proceed by quantizing the circuit Hamiltonian, adopting the standard approach of the second quantization [39] and introducing the creation and annihilation operators for the resonators, \hat{a}_k^\dagger and \hat{a}_k , as well as for the qubit,

$\hat{\sigma}^+$ and $\hat{\sigma}^-$. This leads to the quantized Hamiltonian:

$$\hat{H} = \hbar\omega_q \left(\hat{\sigma}^+ \hat{\sigma}^- + \frac{1}{2} \right) + \hbar \sum_{k=1}^2 \omega_{R_k} \left(\hat{a}_k^\dagger \hat{a}_k + \frac{1}{2} \right) + \hbar \sum_{k=1}^2 g_k (\hat{a}_k^\dagger \hat{\sigma}^- + \hat{a}_k \hat{\sigma}^+) + \hbar\kappa (\hat{a}_1^\dagger \hat{a}_2 + \hat{a}_1 \hat{a}_2^\dagger), \quad (3)$$

where $\hbar\omega_q = \sqrt{8E_C\tilde{E}_J} - E_C$ is the qubit frequency, and $\omega_{R_k} = 1/\sqrt{C_{R_k}L_{R_k}}$ the resonators ones. The Hamiltonian is valid when $\min\{\omega_q, \omega_{R_k}\} \gg \max\{g_k, \kappa\}$ after applying the rotating-wave approximation, where the resonator-qubit and resonator-resonator coupling strengths read

$$g_k = -\frac{1}{\hbar} \frac{C_{q_k}}{\sqrt{C_T C_{R_k}}} \left(2E_C \tilde{E}_J \epsilon_{R_k}^2 \right)^{1/4}, \quad (4a)$$

$$\kappa = \frac{C_{q_1} C_{q_2}}{C_T \sqrt{C_{R_1} C_{R_2}}} \frac{\sqrt{\epsilon_{R_2} \epsilon_{R_1}}}{\hbar}, \quad (4b)$$

with $E_C = e^2/2C_T$ the qubit charging energy and $\epsilon_{R_k} = \hbar\omega_{R_k}/2$ the zero-point energy of the k th resonator.

The collateral coupling strength κ depends on the different parameters of the electronic elements of the superconducting chip, since the Josephson junction capacitance is encoded in C_T . While it does not depend on the physical distance between the two resonators, it scales as $C_{q_1} C_{q_2}$, and acts as a correction to the dynamics composed of the direct resonator-qubit coupling C_{q_k} only. As for their relative amplitude, let us consider the following parameters for the capacitances and inductances [39]: $C_{R_k} = 4C_T = 400.0$ fF and $L_{R_k} = 0.8$ nH correspond to a frequency $\omega_{R_k}/2\pi \approx 8.9$ GHz, coupling capacitances of $C_{q_k} = C_{R_k}/50 \approx 8.0$ fF, and a Josephson energy $E_J = 50E_C$. This leads to the coupling values $g_k/2\pi \approx -139.7$ MHz and $\kappa/2\pi \approx 7.1$ MHz, so the ratio between the collateral resonator-resonator coupling and the direct resonator-qubit coupling is of the order $\kappa/g_k \sim 20$. Even without a detailed analysis of the dynamics, such a correction cannot be neglected in the context of high-fidelity on-resonance operations, where the last term in Eq. (3) becomes relevant. But what is more, as we shall now see, it can even induce an idling point for the resonator dynamics.

III. ON-RESONANCE IDLING POINT

The effect of the collateral coupling κ on the circuit dynamics can be appreciated in the population evolution for state $|Ng0\rangle = |N\rangle_{R_1} |g\rangle_Q |0\rangle_{R_2}$ presented in Fig. 2. After being initialized in that state, the resonators are put at the same frequency, and the excitation starts oscillating back and forth between resonator R_1 and R_2 , at a frequency which characterizes the resonator-resonator effective coupling strength $g_{R_1 R_2}^{\text{eff}}$ [45–49]. As it can be seen from

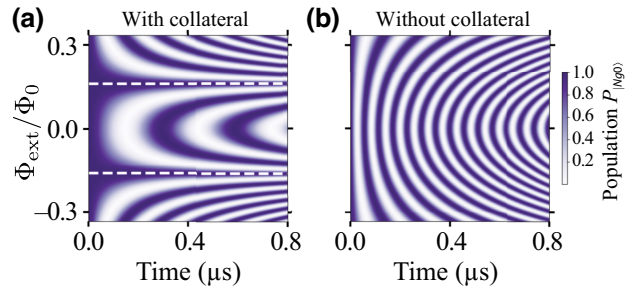


FIG. 2. Dynamics of the population $P(t) = |\langle Ng0 | \psi(t) \rangle|^2$ of state $|Ng0\rangle = |N\rangle_{R_1} |g\rangle_Q |0\rangle_{R_2}$ (considering that the system is initially in that state), as a function of time and the qubit external flux (a) simulating the full Hamiltonian (3) with idling point at $\Phi_{\text{ext}}/\Phi_0 \approx 0.16$, and (b) canceling artificially the collateral term ($\kappa = 0$, as it is usually assumed [28,43,44]). Simulations realized with $C_{R_k} = 4C_T = 400.0$ fF, $L_{R_k} = 0.8$ nH, $C_{q_k} = C_{R_k}/50$ and $E_J = 70E_C$. Note that for flux values in the interval $\Phi_{\text{ext}}/\Phi_0 \in [-1/3, 1/3]$, one has $\tilde{E}_J \geq 70E_C$, which guarantees to operate in the transmon regime ($\tilde{E}_J \gg E_C$).

comparing the dynamics with and without collateral term [(a) and (b), respectively], this extra contribution alters dramatically the resonator-resonator coupling.

For the set of parameters considered in Fig. 2, the resonator-resonator effective coupling between resonators cancels for $\Phi_{\text{ext}} \approx \pm 4\Phi_0/25$, and an idling point emerges: the population remains blocked in state $|Ng0\rangle$ [dashed white lines in Fig. 2(a)]. This corresponds to a cutoff frequency for the qubit, at which the transfer of information between the resonators is prevented. The effect of the collateral coupling on the circuit dynamics is thus particularly striking in this regime, despite its small relative weight as compared to the direct resonator-qubit coupling ($g_k/\kappa \sim 20$). As we shall see now, this stems from the fact that while the collateral coupling depends on κ only, the effective interaction between the resonators can be tuned independently through the different circuit parameters, so the two interactions can cancel.

The emergence of this idling point is more easily understood from the effective dynamics. Let us now focus on the case where resonators have the same frequency, $\omega_{R_1} = \omega_{R_2} = \omega_R$. We enter the dispersive regime for the qubit-mediated interaction by choosing a large detuning $\Delta = \omega_q - \omega_R$, that is, $|\Delta| \gg g_{1,2}$. Since the qubit remains in its ground state for all the evolution, and assuming the rotating wave approximation, we obtain the effective Hamiltonian, now tracing over the qubit degree of freedom

$$H_{\text{eff}} = \hbar \sum_{n=1}^2 \eta_n \hat{a}_n^\dagger \hat{a}_n + \hbar g_{R_1 R_2}^{\text{eff}} \left(\hat{a}_1 \hat{a}_2^\dagger + \hat{a}_1^\dagger \hat{a}_2 \right), \quad (5)$$

with $\eta_n = g_n^2/\Delta$, and where the first and second terms stand for the free Hamiltonian, which describes the energy shifts, but no population exchange. The third

term describes the resonator-resonator coupling, $g_{R_1 R_2}^{\text{eff}} = g_1 g_2 / \Delta + \kappa$: it is a combination of the collateral term κ with the qubit-mediated interaction, characterized by the coupling $g_1 g_2 / \Delta$. The idling point corresponds to the situation where these two contributions cancel, $\Delta = -g_1 g_2 / \kappa$ in the dispersive regime discussed here. In that case, only the free Hamiltonian remains, which does not allow for information transfer between the resonators. In terms of external flux, this condition translates into (see Appendix B)

$$\Phi_{\text{ext}}/\Phi_0 = \frac{1}{\pi} \arccos \left(\frac{(\kappa C_{R_k} C_T (E_C + \hbar \omega_{R_k}))^2}{E_C E_J (4\kappa C_{R_k} C_T + C_{q_k}^2 \omega_{R_k})^2} \right). \quad (6)$$

Note that the existence of the idling point relies on a finite value of the collateral term κ . Indeed, if $\kappa = 0$, the idling point condition (6) imposes $\Phi_{\text{ext}}/\Phi_0 = \pi(2m+1)$ for the external flux, with $m \in \mathbb{N}$. This is satisfied when $E_J = 0$, and consequently $g_k = 0$, which represents a trivial solution where qubit and resonators do not interact at all. On the other hand, the effective Hamiltonian approach results in $\Phi_{\text{ext}}/\Phi_0 \approx 0.1618$, in excellent agreement with the simulations of the total Hamiltonian presented in Fig. 2(a).

It is worthwhile to mention that the idling point has been experimentally investigated in coupled qubit systems where the parasitic interaction is present [33,49,50]. However, we stress that the idling points observed in these works have been attributed to the existence of the direct (capacitive parasitic) coupling. In the case of superconducting resonators, because the direct coupling is negligible due to the physical distance between them, different strategies have been elaborated to induce an idling point [43,51,52]. Our results show that the collateral effect can be equally used for resonators, to establish the idling point even when no direct parasitic interaction between the resonators is present. The most dramatic consequence of the collateral interaction is the capacity to put on hold the whole quantum dynamics, despite the relatively small amplitude of this term (see Fig. 1). Let us now demonstrate the efficiency of this interaction as a quantum control over the dynamics by using it to generate high-fidelity NOON states between the microwave resonators.

IV. NOON STATES

The idling point resulting from the collateral term κ in turn allows for the generation of specific states, such as NOON states. These two-mode highly entangled state of the form $|\text{NOON}\rangle = 1/\sqrt{2}(|Ng0\rangle + |0gN\rangle)$ are of interest for testing Bell-type inequalities [53] and bring opportunities to explore quantum communication protocols [54]. Their generation in superconducting qubits has been investigated [43,51,52], yet the absence of idling point or state-selective interaction makes the process challenging.

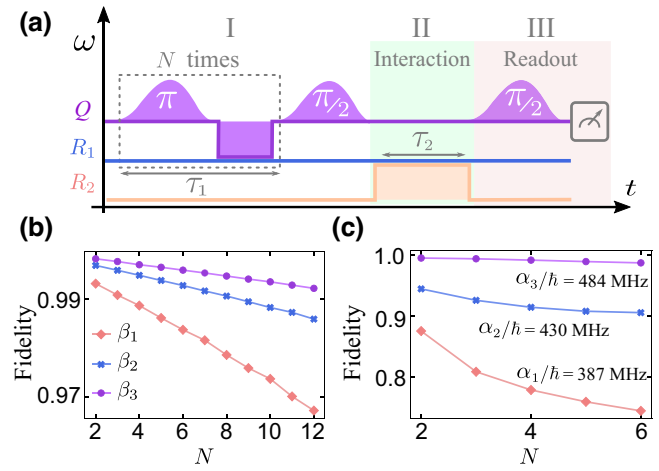


FIG. 3. (a) Pulse sequence to generate the NOON states following our protocol. Step (I): the state in Eq. (7) is prepared. Step (II): the interaction between resonators generates state (8). Step (III): a readout is applied on the qubit to obtain the final states from Eqs. (11) and (12). (b) Fidelity as a function of the number of excitations N . The fidelity increases when the effective limit $C_{q_k} \ll C_{R_k}$ is increasingly satisfied. The parameters used are $C_{R_k} = 4C_T = 400.0 \text{ fF}$, $L_{R_k} = 0.8 \text{ nH}$, and $E_J = 70E_C$, considering the cases $\beta_1 = C_{q_k} = C_{R_k}/50$, $\beta_2 = C_{q_k} = C_{R_k}/75$, and $\beta_3 = C_{q_k} = C_{R_k}/100$, respectively. For (b) a Fock space of dimension $\mathcal{D} = 20$ for each resonator was used. (c) Fidelity when the transmon is treated as a four-level system [56], for three different anharmonicities with a coupling proportional to β_3 . Here we used a Fock space with dimension $\mathcal{D} = 15$ for the resonators.

Let us now describe the protocol to generate efficiently NOON states based on the idling point. First we prepare the system in state $|Ng0\rangle$, by putting qubit R_1 on resonance with qubit Q (but not with R_2), so that the excitation created in the atom with a π pulse is transferred to the first resonator. This operation is repeated N times, which takes a time $\tau_1 \propto N$, see Fig. 3(a). We then apply a $\pi/2$ pulse on Q to generate the following superposition state:

$$|\psi(\tau_1)\rangle = (\mathbb{1}_{R_1} \otimes \pi/2 \otimes \mathbb{1}_{R_2}) |Ng0\rangle = \frac{1}{\sqrt{2}} (|Ng0\rangle + |Ne0\rangle), \quad (7)$$

with $\mathbb{1}_{R_k}$ the identity matrix for the k th resonator. Finally, the system is let to evolve according to Hamiltonian (3) by setting the two resonators on resonance, and the qubit to the idling frequency given by Eq. (6). After an interaction time $\tau_2 = \pi/[2(\kappa - g_1 g_2 / \Delta)]$, where $(\kappa - g_1 g_2 / \Delta)$ is the effective coupling between the resonators when the qubit is in the excited state, the component $|Ne0\rangle$ of the state has changed into $|0eN\rangle$. Yet the component $|Ng0\rangle$ with the qubit in the ground remains unchanged, since the information can flow between the resonators only when the qubit is in state $|e\rangle$. This particular dynamics is a consequence of the state-dependence of the idling point, and the system

ends in state

$$|\psi(\tau_2)\rangle = \frac{1}{\sqrt{2}} (|Ng0\rangle + e^{i\theta} |0eN\rangle), \quad (8)$$

where $e^{i\theta}$ is a dynamical relative phase. Then, we apply a second $\pi/2$ pulse on the qubit, sending the system into

$$|\psi_{\text{out}}\rangle = \frac{1}{2} (|Ng0\rangle + e^{i\theta} |0gN\rangle) + \frac{1}{2} (|Ne0\rangle - e^{i\theta} |0eN\rangle). \quad (9)$$

Finally we perform a measurement of the qubit state, given the positive operator valued measures $\{M_0 = \mathbb{1}_{R_1} \otimes |g\rangle\langle g| \otimes \mathbb{1}_{R_2}, M_1 = \mathbb{1}_{R_1} \otimes |e\rangle\langle e| \otimes \mathbb{1}_{R_2}\}$ such that

$$|\Psi_i\rangle = \frac{M_i |\psi_{\text{out}}\rangle}{\sqrt{\langle\psi_{\text{out}}| M_i |\psi_{\text{out}}\rangle}}, \quad i \in \{0, 1\}. \quad (10)$$

The possible outputs of this measurement are, with equal probability, the following system states

$$|\Psi_0\rangle = \frac{1}{\sqrt{2}} (|Ng0\rangle + e^{i\theta} |0gN\rangle), \quad (11)$$

$$|\Psi_1\rangle = \frac{1}{\sqrt{2}} (|Ne0\rangle - e^{i\theta} |0eN\rangle). \quad (12)$$

Therefore, by monitoring the measured qubit state, $|g\rangle$ or $|e\rangle$, we obtain a NOON state, with a relative phase, which can be eliminated [22]. Hence, our protocol is able to deterministically generate maximally entangled states between the resonators.

The fidelity of our protocol is quantified using the definition $F(\rho, \sigma) = \text{Tr} [\sqrt{\rho^{1/2} \sigma \rho^{1/2}}]$ [55], where ρ represents the protocol output state with corrected phase and σ the ideal NOON state. The high fidelity of the NOON states obtained with this protocol is illustrated in Fig. 3(b), where the scaling of its fidelity with the photon number N is plotted. The fidelity reduces as N increases, due to the superradiantlike enhancement in the effective coupling. Indeed, when an increasing number N of photons are present in the modes, the validity of dispersive regime approximation is affected, so the dynamics deviates from the ideal one given by the effective Hamiltonian (5). This can be compensated by reducing the qubit resonator g_k , re-entering the dispersive regime, as can be observed in Fig. 3(b). For the parameters under consideration, our protocol is able to generate post-selection NOON states with a fidelity over 99%.

The advantage of our protocol with respect to the previous proposal in Ref. [43] can be found in the number of steps required to generate a NOON state with N excitations. Indeed, as depicted in Fig. 3(a), only $2N + 4$ steps are needed to achieve a N -excitation state: $2N$

to generate state $|Ng0\rangle$ and four steps in the $\pi/2 \rightarrow$ interaction time $\rightarrow \pi/2 \rightarrow$ measurement sequence. Differently, the protocol proposed in Ref. [43] requires $4N$ steps, which makes it more prone to errors. The difference in step numbers is particularly advantageous when the number of excitations grows. Our analysis is done by assuming that the whole protocol [circuit in Fig. 3(a)] can be implemented over a time shorter than the relaxation time of the resonators, reminding that the relaxation time of the N th excited states reduces with N [57–60].

Furthermore, because superconducting transmons are artificial (multilevel) atoms instead of pure two-level systems, one has to account for the existence of an anharmonic term in the transmon dynamics. The associated Hamiltonian reads

$$\begin{aligned} \hat{H}_{\text{atom}} = & \hbar \omega_q \hat{b}^\dagger \hat{b} + \frac{\alpha}{2} \hat{b}^\dagger \hat{b}^\dagger \hat{b} \hat{b} + \hbar \sum_{k=1}^2 \omega_{R_k} \left(\hat{a}_k^\dagger \hat{a}_k + \frac{1}{2} \right) \\ & + \hbar \sum_{k=1}^2 g_k (\hat{a}_k^\dagger \hat{b}^- + \hat{a}_k \hat{b}^+) + \hbar \kappa (\hat{a}_1^\dagger \hat{a}_2 + \hat{a}_1 \hat{a}_2^\dagger), \end{aligned} \quad (13)$$

with \hat{b}^\dagger (\hat{b}) the creation (annihilation) operator for the atom, and $\alpha = -E_C$ the anharmonicity energy. In state-of-the-art experiments, the anharmonic frequency $|\alpha|/\hbar$ ranges from weak values of a few tens of MHz ($|\alpha|/\hbar \sim 5 \times 2\pi$ MHz [61]) up to values $|\alpha|/\hbar \sim 250 \times 2\pi$ MHz [62]. As shown in Fig. 3(c), a weaker anharmonicity leads to a reduced fidelity for the NOON states generated. This can be explained by the rising of undesired effects such as residual ZZ parasitic interactions [63,64] and/or population leakage [65], from which the system dynamics suffer substantially. However, larger values of anharmonicity, compatible with recent experiments, allow high-fidelity states to be recovered, even comparable to the one obtained in the two-level approximation.

V. ATOMS IN OPTICAL CAVITIES

Our study opens prospects for a broad class of systems where qubits and resonators are coupled, such as crossed optical cavities [66,67]. For these setups, the collateral interaction between the modes is derived through the classical Hamiltonian $H = (\vec{p} - q\vec{A})^2/(2m) + qU$ of a particle interacting with a radiation field, where \vec{p} , q , and m are the momentum, net charge, and mass of the charged particle—here a valence electron. \vec{A} and U represent the vector and scalar potential of the field, respectively. The collateral interaction here stems from the term $q^2 \vec{A}^2/(2m)$, as already identified by Fermi [42], yet then neglected in optical cavity experiments. Moving to SI units and quantizing

the vector potential \vec{A} , we obtain

$$\vec{A} = \sum_{k,\lambda} \left(\frac{\hbar}{2\epsilon_0 \omega_k V} \right)^{1/2} \left(\hat{a}_{k\lambda}(t) e^{i\vec{k}\cdot\vec{r}} \hat{e}_{k\lambda} + \hat{a}_{k\lambda}^\dagger(t) e^{-i\vec{k}\cdot\vec{r}} \hat{e}_{k\lambda}^* \right). \quad (14)$$

This leads to the interaction between two modes of frequency ω_1 and ω_2 [42]: $\kappa_c = q^2/4m\epsilon_0 V\sqrt{\omega_1\omega_2}$, with ϵ_0 the vacuum permittivity and V the volume in which the vector potential is confined.

Let us now consider that these two cavities are resonant with the transition of the atom, which mediates the interaction between them (frequency $\omega_a = \omega_1 = \omega_2$). The atom-mode coupling is then given by $g = d\sqrt{\omega_a/2\epsilon_0\hbar V}$, with d the electric dipole moment of the transition. The transition linewidth being given by $\Gamma = \omega_a^3 d^2 / 3\pi\epsilon_0\hbar c^3$, with c the light velocity, we obtain $g/\kappa_c = m\epsilon_0\sqrt{24\pi Vc^3\Gamma}/q^2$. For the most recent setups of crossed optical cavities [66] with a mode volume $V \sim 10^4 \mu\text{m}^2$, the collateral term is several orders of magnitude smaller than the coupling g for a MHz transition linewidth. Nevertheless, for a mHz linewidth such as those explored for clocks [68], we obtain a ratio $g/\kappa_c \approx 40$. Then, as in the case of the superconducting circuit, the collateral coupling may have a drastic effect on the dynamics, allowing for an idling point and thus an additional mechanism to operate quantum gates, for example. Indeed, while parasitic coupling between resonators in superconducting circuits do allow idling points to be achieved, such couplings are, in principle, absent from optical cavity setups.

VI. CONCLUSION AND PROSPECTS

We have thus discussed how a collateral interaction arises when a qubit is used to mediate an interaction between the resonators of a superconducting circuit, as one transforms the Lagrangian of the system into a Hamiltonian to obtain dynamical equations. Despite the fact that the interaction has an amplitude much weaker than the direct resonator-qubit coupling, it is able to induce an idling point between the resonators: even for resonant resonators, it prevents the flow of information between them. However, the state-dependent nature of the idling point actually offers an alternative control parameter for the system, which allowed us to propose a scheme for a fast and high-fidelity generation of maximally entangled NOON

states between the superconducting resonators. Equally present in crossed optical cavities interacting through cold atoms, the effect could provide an alternative control parameter to operate quantum gates in these setups as well.

The present work, applicable to grounded couplers, is complementary to the approach of floating couplers, which used to bring additional control parameters and thus more flexibility in the range of parameters achievable [69], as well as long-range interactions among the circuits elements [70]. The collateral effect thus brings another tool of control for complex integrated circuits, which can also be extended to other kinds of superconducting hybrid platforms. Other promising platforms able to exploit collateral coupling are systems of semiconductor quantum dots in circuit waveguide quantum electrodynamics [71], and phonon-mediated interacting superconducting qubits coupled to a piezoelectric resonator [72], for instance. More generally, it should apply to any system with a Lagrangian equivalent to the one presented in Eq. (1).

ACKNOWLEDGMENTS

The authors acknowledge the financial support of the São Paulo Research Foundation (FAPESP) (Grants No. 2018/15554-5, No. 2019/22685-1, No. 2019/13143-0, No. 2019/11999-5, No. 2021/10224-0, and No. 2022/12382-4) and of the Brazilian CNPq (Conselho Nacional de Desenvolvimento Científico e Tecnológico), Grants No. 130267/2022-8, No. 313886/2020-2, No. 465469/2014-0, and No. 311612/2021-0.

APPENDIX A: SYSTEM DESCRIPTION

Consider the superconducting circuit of two resonators and a single transmon qubit where capacitive parasitic interaction introduce the capacitance $C_{R_1 R_2}$ between the resonators, as sketched in Fig. 4. The Lagrangian of the system has the general form

$$L = \frac{1}{2} \vec{\phi}^T \hat{C} \vec{\phi} - U(\phi_J, \phi_{R_1}, \phi_{R_2}), \quad (\text{A1})$$

where $\vec{\phi}^T = (\dot{\phi}_J, \dot{\phi}_{R_1}, \dot{\phi}_{R_2})$ and \hat{C} is the capacitance matrix. Then, the capacitance matrix can be derived from Eq. (A1), using the conjugate momentum of the node flux $q_k = \partial L(\vec{\phi}, \vec{\dot{\phi}})/\partial \dot{\phi}_k$, and one obtains

$$\hat{C} = \begin{pmatrix} C_T + C_{q_1} + C_{q_2} & -C_{q_1} & -C_{q_2} \\ -C_{q_1} & C_{R_1} + C_{q_1} + C_{R_1 R_2} & -C_{R_1 R_2} \\ -C_{q_2} & -C_{R_1 R_2} & C_{R_2} + C_{q_2} + C_{R_1 R_2} \end{pmatrix}. \quad (\text{A2})$$

Switching to the Hamiltonian approach we get

$$H = \frac{1}{2} \vec{q}^T \hat{C}^{-1} \vec{q} + U(\phi_J, \phi_{R_1}, \phi_{R_2}), \quad (\text{A3})$$

where $U(\vec{\phi}) = 1/2L_{R_1}\phi_{R_1}^2 + 1/2L_{R_2}\phi_{R_2}^2 - \tilde{E}_J \cos(\phi_J/\phi_0)$, $\vec{q}^T = (q_J, q_{R_1}, q_{R_2})$, and \hat{C}^{-1} is the inverse of the

capacitance matrix, which induces the collateral interaction between the resonators. Indeed, if one then assumes that $C_T \gg C_{q_k}$ and $C_{R_k} \gg C_{q_k}$, one can approximate the terms $C_T + C_{q_1} + C_{q_2} \approx C_T$ and $C_{R_k} + C_{q_k} \approx C_{R_k}$ in Eq. (A2), to obtain the following inverse capacitance matrix:

$$\hat{C}^{-1} \approx \begin{pmatrix} \frac{1}{C_T} & \frac{C_{q_1}C_{R_2}}{\text{Det}(\hat{C})} & \frac{C_{q_2}C_{R_1}}{\text{Det}(\hat{C})} \\ \frac{C_{q_1}C_{R_2}}{\text{Det}(\hat{C})} & \frac{C_T(C_{R_2} + C_{R_1R_2})}{\text{Det}(\hat{C})} & \frac{C_{q_1}C_{q_2} + C_{R_1R_2}C_T}{\text{Det}(\hat{C})} \\ \frac{C_{q_2}C_{R_1}}{\text{Det}(\hat{C})} & \frac{C_{q_1}C_{q_2} + C_{R_1R_2}C_T}{\text{Det}(\hat{C})} & \frac{C_T(C_{R_1} + C_{R_1R_2})}{\text{Det}(\hat{C})} \end{pmatrix}, \quad (\text{A4})$$

where $\text{Det}(\hat{C}) \approx C_T(C_{R_1}C_{R_2} + C_{R_1R_2}(C_{R_1} + C_{R_2}))$. The charge-charge capacitive coupling between the resonators reads

$$\frac{1}{\text{Det}(\hat{C})}(C_{q_1}C_{q_2} + C_{R_1R_2}C_T)q_{R_1}q_{R_2}. \quad (\text{A5})$$

Note that, in the regime where the physical distance between the resonators is large enough, the direct capacitive coupling represented in Fig. 4 vanishes ($C_{R_1R_2} \rightarrow 0$) and the resonators coupling in Eq. (A5) has only the collateral contribution due to the capacitance network

$$\frac{C_{q_1}C_{q_2}}{C_{R_1}C_{R_2}C_T}q_{R_1}q_{R_2}. \quad (\text{A6})$$

In our system description, we are only interested in studying the effect of the collateral interaction to the quantum dynamics, therefore we do not consider the direct parasitic coupling ($C_{R_1R_2} \rightarrow 0$) and the inverse capacitance matrix

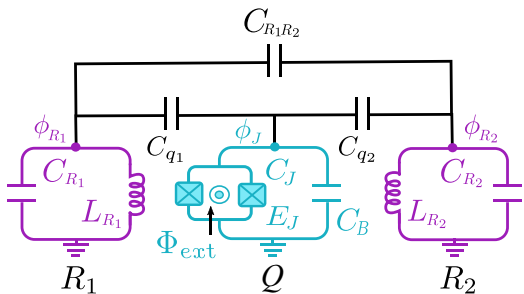


FIG. 4. Schematic representation considering the direct parasitic capacitive interaction $C_{R_1R_2}$.

takes the form

$$\hat{C}^{-1} \approx \begin{pmatrix} \frac{1}{C_T} & \frac{C_{q_1}}{C_{R_1}C_T} & \frac{C_{q_2}}{C_{R_2}C_T} \\ \frac{C_{q_1}}{C_{R_1}C_T} & \frac{1}{C_{R_1}} & \frac{C_{q_1}C_{q_2}}{C_{R_1}C_{R_2}C_T} \\ \frac{C_{q_2}}{C_{R_2}C_T} & \frac{C_{q_1}C_{q_2}}{C_{R_1}C_{R_2}C_T} & \frac{1}{C_{R_2}} \end{pmatrix}. \quad (\text{A7})$$

Then, Hamiltonian (A3) reads

$$\begin{aligned} H \approx & \frac{q_J^2}{2C_T} - \tilde{E}_J \cos\left(\frac{\phi_J}{\Phi_0}\right) + \frac{q_{R_1}^2}{2C_{R_1}} + \frac{\phi_{R_1}^2}{2L_{R_1}} + \frac{q_{R_2}^2}{2C_{R_2}} \\ & + \frac{\phi_{R_2}^2}{2L_{R_2}} + \frac{C_{q_1}}{C_{R_1}C_T}q_Jq_{R_1} + \frac{C_{q_2}}{C_{R_2}C_T}q_Jq_{R_2} \\ & + \frac{C_{q_1}C_{q_2}}{C_{R_1}C_{R_2}C_T}q_{R_1}q_{R_2}, \end{aligned} \quad (\text{A8})$$

with the collateral term now becomes explicit. The quantization of the circuit is done through the canonical quantization that consists in turning the functions q and ϕ for their respective operators \hat{q} and $\hat{\phi}$, along with the second quantization approach where the creation and annihilation operators for the resonators are introduced

$$\begin{aligned} \hat{\phi}_{R_k} &= \left(\frac{\hbar Z_{R_k}}{2}\right)^{1/2}(\hat{a}_k + \hat{a}_k^\dagger), \\ \hat{q}_{R_k} &= i\left(\frac{\hbar}{2Z_{R_k}}\right)^{1/2}(\hat{a}_k^\dagger - \hat{a}_k), \end{aligned} \quad (\text{A9})$$

with $Z_{R_k} = \sqrt{L_{R_k}/C_{R_k}}$ the impedance of each resonator. The transmon variables are given by

$$\begin{aligned}\hat{\phi}_J &= \frac{1}{\sqrt{2}} \left(\frac{8E_C}{\tilde{E}_J} \right)^{1/4} (\hat{b} + \hat{b}^\dagger), \\ \hat{q}_J &= -\frac{2ie}{\sqrt{2}} \left(\frac{\tilde{E}_J}{8E_C} \right)^{1/4} (\hat{b} - \hat{b}^\dagger),\end{aligned}\quad (\text{A10})$$

with $E_C = e^2/2C_T$. Since the Josephson energy \tilde{E}_J is much larger than the capacitance energy E_C , one can expand and approximate the contribution of the Josephson junction to the Hamiltonian as [32]

$$\tilde{E}_J \cos\left(\frac{\hat{\phi}_J}{\Phi_0}\right) \approx \tilde{E}_J \left[\mathbb{I} - \frac{1}{2} \left(\frac{\hat{\phi}_J}{\Phi_0} \right)^2 + \frac{1}{4!} \left(\frac{\hat{\phi}_J}{\Phi_0} \right)^4 \right]. \quad (\text{A11})$$

Eventually, one gets

$$\begin{aligned}H &= \hbar\omega_q \left(\hat{b}^\dagger \hat{b} + \frac{\mathbb{I}}{2} \right) - \frac{E_C}{2} \hat{b}^\dagger \hat{b}^\dagger \hat{b} \hat{b} + \hbar\omega_{R_1} \left(\hat{a}_1^\dagger \hat{a}_1 + \frac{\mathbb{I}}{2} \right) \\ &\quad + \hbar\omega_{R_2} \left(\hat{a}_2^\dagger \hat{a}_2 + \frac{\mathbb{I}}{2} \right) + \hbar g_1 (\hat{b} - \hat{b}^\dagger) (\hat{a}_1^\dagger - \hat{a}_1) \\ &\quad + \hbar g_2 (\hat{b} - \hat{b}^\dagger) (\hat{a}_2^\dagger - \hat{a}_2) - \hbar\kappa (\hat{a}_1^\dagger - \hat{a}_1) (\hat{a}_2^\dagger - \hat{a}_2),\end{aligned}\quad (\text{A12})$$

where $\hbar\omega_q = \sqrt{8E_C\tilde{E}_J} - E_C$ and $\omega_{R_k} = 1/\sqrt{C_{R_k}L_{R_k}}$ are the qubit and resonators frequencies, respectively. The coupling strengths read

$$g_k = -\frac{1}{\hbar} \frac{C_{q_k}}{\sqrt{C_T C_{R_k}}} \left(2E_C \tilde{E}_J \epsilon_{R_k}^2 \right)^{1/4}, \quad (\text{A13a})$$

$$\kappa = \frac{C_{q_1} C_{q_2}}{C_T \sqrt{C_{R_1} C_{R_2}}} \frac{\sqrt{\epsilon_{R_2} \epsilon_{R_1}}}{\hbar}, \quad (\text{A13b})$$

with $\epsilon_{R_k} = \hbar\omega_{R_k}/2$ the zero-point energy of the k th resonator. In general, the energy in the superconducting device has the form [4]

$$\tilde{E}_J = (E_{J_1} + E_{J_2}) \cos\left(\pi \frac{\Phi_{\text{ext}}}{\Phi_0}\right) \sqrt{1 + d^2 \tan^2\left(\pi \frac{\Phi_{\text{ext}}}{\Phi_0}\right)}, \quad (\text{A14})$$

with $d = E_{J_1} - E_{J_2}/E_{J_1} + E_{J_2}$ the asymmetry parameter. Considering two Josephson junctions with the same associated energy ($d = 0$), the energy rewrites $\tilde{E}_J = \tilde{E}_J(\Phi_{\text{ext}}) = 2E_J |\cos(\pi\Phi_{\text{ext}}/\Phi_0)|$. Equation (3) in the main text is

obtained from Eq. (A12) using the second-level approximation $\hat{b}^\dagger := \hat{\sigma}^+$, $\hat{b} := \hat{\sigma}^-$, and neglecting the nonconserving terms of the form $\hat{b}^\dagger \hat{a}_j^\dagger$, $\hat{b} \hat{a}_j$, $\hat{a}_i \hat{a}_j$, and $\hat{a}_i^\dagger \hat{a}_j^\dagger$ with $j \neq i \in \{1, 2\}$.

It is worth mentioning that the main contribution from parasitic interactions, which leads to $C_{R_1 R_2} \neq 0$, is a change in the Hamiltonian in Eq. (A12) of the form

$$H' = H + \hbar g_{\text{par}} (\hat{a}_1^\dagger - \hat{a}_1) (\hat{a}_2^\dagger - \hat{a}_2). \quad (\text{A15})$$

As conclusion, the parasitic interaction will affect only the regime of parameters of the idling point, since this extra interaction can be easily accounted for by a suitable redefinition of the coupler frequency.

APPENDIX B: EFFECTIVE HAMILTONIAN AND IDLING POINT

Consider resonators on resonance $\omega_{R_1} = \omega_{R_2} = \omega_R$, then the detuning of the qubit is the same for both resonators $\Delta = \omega_q - \omega_R$. The interaction Hamiltonian is given by the transformation $H_{\text{in}}(t) = e^{iH_{\text{fs}}t/\hbar} H_I e^{-iH_{\text{fs}}t/\hbar}$, where $H_{\text{fs}} = \hbar\omega_q \hat{\sigma}^+ \hat{\sigma}^- + \hbar\omega_{R_1} \hat{a}_1^\dagger \hat{a}_1 + \hbar\omega_{R_2} \hat{a}_2^\dagger \hat{a}_2$ describes the local contribution of each element in the system. $H_I = \hbar g_1 (\hat{\sigma}^- \hat{a}_1^\dagger + \hat{\sigma}^+ \hat{a}_1) + \hbar g_2 (\hat{\sigma}^- \hat{a}_2^\dagger + \hat{\sigma}^+ \hat{a}_2) + \hbar\kappa (\hat{a}_1^\dagger \hat{a}_2 + \hat{a}_1 \hat{a}_2^\dagger)$ represents the interactions transmon-resonator and resonator-resonator, therefore it also encodes the collateral contribution to the dynamics. After some algebra we obtain

$$\begin{aligned}H_{\text{in}}(t) &= \hbar g_1 (e^{i\Delta t} \sigma^+ \hat{a}_1 + e^{-i\Delta t} \sigma^- \hat{a}_1^\dagger) \\ &\quad + \hbar g_2 (e^{i\Delta t} \sigma^+ \hat{a}_2 + e^{-i\Delta t} \sigma^- \hat{a}_2^\dagger) \\ &\quad + \hbar\kappa (\hat{a}_1^\dagger \hat{a}_2 + \hat{a}_1 \hat{a}_2^\dagger).\end{aligned}\quad (\text{B1})$$

The effective Hamiltonian is obtained by eliminating the fast rotating terms (rotating-wave approximation) assuming that $|\Delta| \gg g_k$:

$$\begin{aligned}H_{\text{eff}}(t) &\approx \frac{1}{i\hbar} H_{\text{in}}(t) \int_0^t H_{\text{in}}(t') dt' \\ &= \hbar\kappa (\hat{a}_1^\dagger \hat{a}_2 + \hat{a}_1 \hat{a}_2^\dagger) \\ &\quad + \frac{\hbar g_1^2}{\Delta} (\hat{\sigma}^+ \hat{\sigma}^- \hat{a}_1 \hat{a}_1^\dagger - \hat{\sigma}^- \hat{\sigma}^+ \hat{a}_1^\dagger \hat{a}_1) \\ &\quad + \frac{\hbar g_1 g_2}{\Delta} (\hat{\sigma}^+ \hat{\sigma}^- \hat{a}_1 \hat{a}_2^\dagger - \hat{\sigma}^- \hat{\sigma}^+ \hat{a}_1^\dagger \hat{a}_2) \\ &\quad + \frac{\hbar g_2^2}{\Delta} (\hat{\sigma}^+ \hat{\sigma}^- \hat{a}_2 \hat{a}_2^\dagger - \hat{\sigma}^- \hat{\sigma}^+ \hat{a}_2^\dagger \hat{a}_2) \\ &\quad + \frac{\hbar g_1 g_2}{\Delta} (\hat{\sigma}^+ \hat{\sigma}^- \hat{a}_2 \hat{a}_1^\dagger - \hat{\sigma}^- \hat{\sigma}^+ \hat{a}_2^\dagger \hat{a}_1),\end{aligned}\quad (\text{B2})$$

which can be rewritten as Eq. (5) from the main text. This expression can in turn be used to determine the

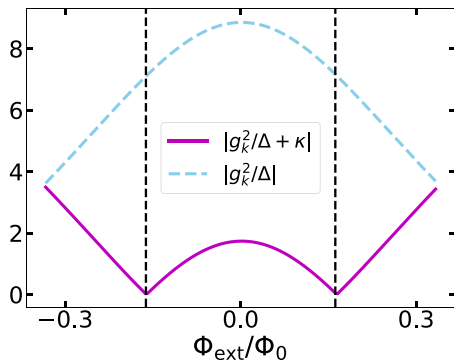


FIG. 5. Absolute value of the effective coupling as a function of the external flux, with and without κ . Vertical lines corresponds to the analytical formula (6).

idling point, where the resonators stop exchanging excitations. This occurs when the effective coupling between the resonators is null with the qubit in state $|g\rangle$:

$$\frac{g_k^2}{\Delta} + \kappa = 0, \quad (\text{B3})$$

where we have used that $g_1 = g_2 = g_k$. This leads to the following conditions on the external flux for the dynamics to be static:

$$\begin{aligned} 0 &\stackrel{1}{=} \frac{1}{\hbar C_T C_{R_k}} \frac{\left(2E_C \tilde{E}_J \epsilon_{R_k}^2\right)^{\frac{1}{2}}}{\sqrt{8E_C \tilde{E}_J - E_C - \hbar\omega_{R_k}}} + \kappa \\ 0 &\stackrel{2}{=} \frac{1}{\hbar C_T C_{R_k}} \left(2E_C \tilde{E}_J \epsilon_{R_k}^2\right)^{\frac{1}{2}} + \kappa \left(\sqrt{8E_C \tilde{E}_J} - E_C - \hbar\omega_{R_k}\right) \\ 0 &\stackrel{3}{=} \frac{2\kappa C_T C_{R_k} (E_C + \hbar\omega_{R_k})}{\sqrt{2E_C} (C_{q_k}^2 \omega_{R_k} + 4\kappa C_T C_{R_k})} - \sqrt{\tilde{E}_J}. \end{aligned} \quad (\text{B4})$$

Using the last equation, we obtain expression (6) presented in the main text.

In Fig. 5 we present the effective coupling as a function of the external flux, with and without collateral interaction: this illustrates the necessity of a finite collateral coupling κ to generate the idling point.

and fixed transition frequencies, *Phys. Rev. B* **81**, 134507 (2010).

- [4] A. Blais, A. L. Grimsom, S. M. Girvin, and A. Wallraff, Circuit quantum electrodynamics, *Rev. Mod. Phys.* **93**, 025005 (2021).
- [5] F. Arute, *et al.*, Quantum supremacy using a programmable superconducting processor, *Nature* **574**, 505 (2019).
- [6] Y. Wu, *et al.*, Strong Quantum Computational Advantage using a Superconducting Quantum Processor, *Phys. Rev. Lett.* **127**, 180501 (2021).
- [7] K. Zhang, H. Li, P. Zhang, J. Yuan, J. Chen, W. Ren, Z. Wang, C. Song, D.-W. Wang, H. Wang, S. Zhu, G. S. Agarwal, and M. O. Scully, Synthesizing Five-Body Interaction in a Superconducting Quantum Circuit, *Phys. Rev. Lett.* **128**, 190502 (2022).
- [8] P. Zhao, K. Linghu, Z. Li, P. Xu, R. Wang, G. Xue, Y. Jin, and H. Yu, Quantum Crosstalk Analysis for Simultaneous Gate Operations on Superconducting Qubits, *PRX Quantum* **3**, 020301 (2022).
- [9] Y. Xu, J. Chu, J. Yuan, J. Qiu, Y. Zhou, L. Zhang, X. Tan, Y. Yu, S. Liu, J. Li, F. Yan, and D. Yu, High-Fidelity, High-Scalability Two-Qubit Gate Scheme for Superconducting Qubits, *Phys. Rev. Lett.* **125**, 240503 (2020).
- [10] S. Sheldon, E. Magesan, J. M. Chow, and J. M. Gambetta, Procedure for systematically tuning up cross-talk in the cross-resonance gate, *Phys. Rev. A* **93**, 060302 (2016).
- [11] J. A. B. Mates, D. T. Becker, D. A. Bennett, B. J. Dober, J. D. Gard, G. C. Hilton, D. S. Swetz, L. R. Vale, and J. N. Ullom, Crosstalk in microwave SQUID multiplexers, *Appl. Phys. Lett.* **115**, 202601 (2019).
- [12] W. Nuerbolati, Z. Han, J. Chu, Y. Zhou, X. Tan, Y. Yu, S. Liu, and F. Yan, Canceling microwave crosstalk with fixed-frequency qubits, *Appl. Phys. Lett.* **120**, 174001 (2022).
- [13] X. Dai, R. Trappen, R. Yang, S. M. Disseler, J. I. Basham, J. Gibson, A. J. Melville, B. M. Niedzielski, R. Das, D. K. Kim, J. L. Yoder, S. J. Weber, C. F. Hirjibehedin, D. A. Lidar, and A. Lupascu, Optimizing for periodicity: A model-independent approach to flux crosstalk calibration for superconducting circuits (2022), *ArXiv:2211.01497*.
- [14] V. Tripathi, H. Chen, M. Khezri, K.-W. Yip, E. Levenson-Falk, and D. A. Lidar, Suppression of Crosstalk in Superconducting Qubits using Dynamical Decoupling, *Phys. Rev. Appl.* **18**, 024068 (2022).
- [15] C. Berke, E. Varvelis, S. Trebst, A. Altland, and D. P. DiVincenzo, Transmon platform for quantum computing challenged by chaotic fluctuations, *Nat. Commun.* **13**, 2495 (2022).
- [16] Z.-L. Xiang, S. Ashhab, J. Q. You, and F. Nori, Hybrid quantum circuits: Superconducting circuits interacting with other quantum systems, *Rev. Mod. Phys.* **85**, 623 (2013).
- [17] A. Omran, H. Levine, A. Keesling, G. Semeghini, T. T. Wang, S. Ebadi, H. Bernien, A. S. Zibrov, H. Pichler, and S. Choi, *et al.*, Generation and manipulation of Schrödinger cat states in Rydberg atom arrays, *Science* **365**, 570 (2019).
- [18] M. Mirhosseini, E. Kim, X. Zhang, A. Sipahigil, P. B. Dieterle, A. J. Keller, A. Asenjo-Garcia, D. E. Chang, and O. Painter, Cavity quantum electrodynamics with atom-like mirrors, *Nature* **569**, 692 (2019).

- [19] Z. Wang, H. Li, W. Feng, X. Song, C. Song, W. Liu, Q. Guo, X. Zhang, H. Dong, D. Zheng, H. Wang, and D.-W. Wang, Controllable Switching Between Superradiant and Subradiant States in a 10-Qubit Superconducting Circuit, *Phys. Rev. Lett.* **124**, 013601 (2020).
- [20] B. Marinelli, J. Luo, H. Ren, B. M. Niedzielski, D. K. Kim, R. Das, M. Schwartz, D. I. Santiago, and I. Siddiqi, Dynamically reconfigurable photon exchange in a superconducting quantum processor, arXiv e-prints , ArXiv:2303.03507 (2023).
- [21] M. Hofheinz, E. Weig, M. Ansmann, R. C. Bialczak, E. Lucero, M. Neeley, A. O'Connell, H. Wang, J. M. Martinis, and A. Cleland, Generation of Fock states in a superconducting quantum circuit, *Nature* **454**, 310 (2008).
- [22] M. Hofheinz, H. Wang, M. Ansmann, R. C. Bialczak, E. Lucero, M. Neeley, A. D. O'Connell, D. Sank, J. Wenner, J. M. Martinis, and A. N. Cleland, Synthesizing arbitrary quantum states in a superconducting resonator, *Nature* **459**, 546 (2009).
- [23] C.-P. Yang, Q.-P. Su, S.-B. Zheng, and S. Han, One-step transfer or exchange of arbitrary multipartite quantum states with a single-qubit coupler, *Phys. Rev. B* **92**, 054509 (2015).
- [24] A. Baust, E. Hoffmann, M. Haeberlein, M. J. Schwarz, P. Eder, J. Goetz, F. Wulschner, E. Xie, L. Zhong, F. Quijandría, B. Peropadre, D. Zueco, J.-J. García Ripoll, E. Solano, K. Fedorov, E. P. Menzel, F. Deppe, A. Marx, and R. Gross, Tunable and switchable coupling between two superconducting resonators, *Phys. Rev. B* **91**, 014515 (2015).
- [25] G. M. Reuther, D. Zueco, F. Deppe, E. Hoffmann, E. P. Menzel, T. Weiβl, M. Mariantoni, S. Kohler, A. Marx, E. Solano, R. Gross, and P. Hänggi, Two-resonator circuit quantum electrodynamics: Dissipative theory, *Phys. Rev. B* **81**, 144510 (2010).
- [26] Y. Shen, G. Marchegiani, G. Catelani, L. Amico, A. Q. Liu, W. Fan, and L. C. Kwek, Ghz-like states in the qubit-qudit Rabi model, *SciPost Phys.* **11**, 099 (2021).
- [27] M. Mariantoni, F. Deppe, A. Marx, R. Gross, F. K. Wilhelm, and E. Solano, Two-resonator circuit quantum electrodynamics: A superconducting quantum switch, *Phys. Rev. B* **78**, 104508 (2008).
- [28] H. Wang, M. Mariantoni, R. C. Bialczak, M. Lenander, E. Lucero, M. Neeley, A. D. O'Connell, D. Sank, M. Weides, J. Wenner, T. Yamamoto, Y. Yin, J. Zhao, J. M. Martinis, and A. N. Cleland, Deterministic Entanglement of Photons in Two Superconducting Microwave Resonators, *Phys. Rev. Lett.* **106**, 060401 (2011).
- [29] C. Wang, Y. Y. Gao, P. Reinhold, R. W. Heeres, N. Ofek, K. Chou, C. Axline, M. Reagor, J. Blumoff, K. M. Sliwa, L. Frunzio, S. M. Girvin, L. Jiang, M. Mirrahimi, M. H. Devoret, and R. J. Schoelkopf, A Schrödinger cat living in two boxes, *Science* **352**, 1087 (2016).
- [30] B. R. Johnson, M. D. Reed, A. A. Houck, D. I. Schuster, L. S. Bishop, E. Ginossar, J. M. Gambetta, L. DiCarlo, L. Frunzio, S. M. Girvin, and R. J. Schoelkopf, Quantum non-demolition detection of single microwave photons in a circuit, *Nat. Phys.* **6**, 663 (2010).
- [31] J. J. Garcia Ripoll, *Quantum Information and Quantum Optics with Superconducting Circuits* (Cambridge University Press, Cambridge, England, 2022).
- [32] S. Rasmussen, K. Christensen, S. Pedersen, L. Kristensen, T. Bækkegaard, N. Loft, and N. Zinner, Superconducting Circuit Companion—An Introduction with Worked Examples, *PRX Quantum* **2**, 040204 (2021).
- [33] F. Yan, P. Krantz, Y. Sung, M. Kjaergaard, D. L. Campbell, T. P. Orlando, S. Gustavsson, and W. D. Oliver, Tunable coupling scheme for implementing high-fidelity two-qubit gates, *Phys. Rev. Appl.* **10**, 054062 (2018).
- [34] J. Ku, X. Xu, M. Brink, D. C. McKay, J. B. Hertzberg, M. H. Ansari, and B. L. T. Plourde, Suppression of Unwanted ZZ Interactions in a Hybrid Two-Qubit System, *Phys. Rev. Lett.* **125**, 200504 (2020).
- [35] X. Xu and M. Ansari, ZZ Freedom in Two-Qubit Gates, *Phys. Rev. Appl.* **15**, 064074 (2021).
- [36] X. Xu and M. Ansari, Parasitic-Free Gate: An Error-Protected Cross-Resonance Switch in Weakly Tunable Architectures, *Phys. Rev. Appl.* **19**, 024057 (2023).
- [37] J. Majer, J. M. Chow, J. M. Gambetta, J. Koch, B. R. Johnson, J. A. Schreier, L. Frunzio, D. I. Schuster, A. A. Houck, A. Wallraff, A. Blais, M. H. Devoret, S. M. Girvin, and R. J. Schoelkopf, Coupling superconducting qubits via a cavity bus, *Nature* **449**, 443 (2007).
- [38] R. Barends, J. Kelly, A. Megrant, D. Sank, E. Jeffrey, Y. Chen, Y. Yin, B. Chiaro, J. Mutus, C. Neill, P. O'Malley, P. Roushan, J. Wenner, T. C. White, A. N. Cleland, and J. M. Martinis, Coherent Josephson Qubit Suitable for Scalable Quantum Integrated Circuits, *Phys. Rev. Lett.* **111**, 080502 (2013).
- [39] U. Vool and M. Devoret, Introduction to quantum electromagnetic circuits, *Int. J. Circuit Theory Appl.* **45**, 897 (2017).
- [40] P. Krantz, M. Kjaergaard, F. Yan, T. P. Orlando, S. Gustavsson, and W. D. Oliver, A quantum engineer's guide to superconducting qubits, *Appl. Phys. Rev.* **6**, 021318 (2019).
- [41] C.-P. Yang, Q.-P. Su, and S. Han, Generation of Greenberger-Horne-Zeilinger entangled states of photons in multiple cavities via a superconducting qutrit or an atom through resonant interaction, *Phys. Rev. A* **86**, 022329 (2012).
- [42] E. Fermi, Quantum theory of radiation, *Rev. Mod. Phys.* **4**, 87 (1932).
- [43] F. W. Strauch, K. Jacobs, and R. W. Simmonds, Arbitrary Control of Entanglement Between Two Superconducting Resonators, *Phys. Rev. Lett.* **105**, 050501 (2010).
- [44] Q.-P. Su, C.-P. Yang, and S.-B. Zheng, Fast and simple scheme for generating NOON states of photons in circuit QED, *Sci. Rep.* **4**, 3898 (2014).
- [45] S. A. Caldwell, *et al.*, Parametrically Activated Entangling Gates Using Transmon Qubits, *Phys. Rev. Appl.* **10**, 034050 (2018).
- [46] L. Casparis, M. R. Connolly, M. Kjaergaard, N. J. Pearson, A. Kringhøj, T. W. Larsen, F. Kuemmeth, T. Wang, C. Thomas, and S. Gronin, *et al.*, Superconducting gatemon qubit based on a proximitized two-dimensional electron gas, *Nat. Nanotechnol.* **13**, 915 (2018).
- [47] E. Leonard, M. A. Beck, J. Nelson, B. Christensen, T. Thorbeck, C. Howington, A. Opremcak, I. Pechenezhskiy, K. Dodge, N. Dupuis, M. Hutchings, J. Ku, F. Schlenker, J. Suttle, C. Wilen, S. Zhu, M. Vavilov, B. Plourde, and R. McDermott, Digital Coherent Control of a Superconducting Qubit, *Phys. Rev. Appl.* **11**, 014009 (2019).

- [48] E. Kim, X. Zhang, V. S. Ferreira, J. Bunker, J. K. Iverson, A. Sipahigil, M. Bello, A. González-Tudela, M. Mirhosseini, and O. Painter, Quantum Electrodynamics in a Topological Waveguide, *Phys. Rev. X* **11**, 011015 (2021).
- [49] C.-K. Hu, J. Yuan, B. A. Veloso, J. Qiu, Y. Zhou, L. Zhang, J. Chu, O. Nurbolat, L. Hu, J. Li, Y. Xu, Y. Zhong, S. Liu, F. Yan, D. Tan, R. Bachelard, A. C. Santos, C. J. Villas-Boas, and D. Yu, Conditional coherent control with superconducting artificial atoms, arXiv e-prints , ArXiv:2203.09791 (2022).
- [50] X. Li, T. Cai, H. Yan, Z. Wang, X. Pan, Y. Ma, W. Cai, J. Han, Z. Hua, X. Han, Y. Wu, H. Zhang, H. Wang, Y. Song, L. Duan, and L. Sun, Tunable Coupler for Realizing a Controlled-Phase Gate with Dynamically Decoupled Regime in a Superconducting Circuit, *Phys. Rev. Appl.* **14**, 024070 (2020).
- [51] S. T. Merkel and F. K. Wilhelm, Generation and detection of NOON states in superconducting circuits, *New J. Phys.* **12**, 093036 (2010).
- [52] R. Sharma and F. W. Strauch, Quantum state synthesis of superconducting resonators, *Phys. Rev. A* **93**, 012342 (2016).
- [53] C. F. Wildfeuer, A. P. Lund, and J. P. Dowling, Strong violations of Bell-type inequalities for path-entangled number states, *Phys. Rev. A* **76**, 052101 (2007).
- [54] J.-W. Pan, Z.-B. Chen, C.-Y. Lu, H. Weinfurter, A. Zeilinger, and M. Żukowski, Multiphoton entanglement and interferometry, *Rev. Mod. Phys.* **84**, 777 (2012).
- [55] M. A. Nielsen and I. L. Chuang, *Quantum Computation and Quantum Information: 10th Anniversary Edition* (Cambridge University Press, New York, NY, USA, 2011), 10th ed.
- [56] For the case of highly anharmonic transmons, due to the dispersive resonator-qubit coupling regime, population leakage from the four-level subspace $\{|0\rangle, |1\rangle, |2\rangle, |3\rangle\}$ of the transmon to higher-excited state $|n \geq 4\rangle$ is significantly suppressed, which means that all coherent error due to population leakage from qubit subspace $\{|0\rangle, |1\rangle\}$ is being taken into account in our analysis with a four-level transmon atom. In fact, by numerical and exact simulations of the dynamics we support such a result by finding maximum population $|\langle 3 | \rho(t) | 3 \rangle| < 3 \times 10^{-4}$ for any α and N considered in Fig. 3(c).
- [57] R. Lutchyn, L. Glazman, and A. Larkin, Quasiparticle decay rate of Josephson charge qubit oscillations, *Phys. Rev. B* **72**, 014517 (2005).
- [58] G. Catelani, R. J. Schoelkopf, M. H. Devoret, and L. I. Glazman, Relaxation and frequency shifts induced by quasiparticles in superconducting qubits, *Phys. Rev. B* **84**, 064517 (2011).
- [59] A. P. Sears, A. Petrenko, G. Catelani, L. Sun, H. Paik, G. Kirchmair, L. Frunzio, L. I. Glazman, S. M. Girvin, and R. J. Schoelkopf, Photon shot noise dephasing in the strong-dispersive limit of circuit QED, *Phys. Rev. B* **86**, 180504 (2012).
- [60] M. J. Peterer, S. J. Bader, X. Jin, F. Yan, A. Kamal, T. J. Gudmundsen, P. J. Leek, T. P. Orlando, W. D. Oliver, and S. Gustavsson, Coherence and Decay of Higher Energy Levels of a Superconducting Transmon Qubit, *Phys. Rev. Lett.* **114**, 010501 (2015).
- [61] P. Winkel, K. Borisov, L. Grünhaupt, D. Rieger, M. Specker, F. Valenti, A. V. Ustinov, W. Wernsdorfer, and I. M. Pop, Implementation of a Transmon Qubit Using Superconducting Granular Aluminum, *Phys. Rev. X* **10**, 031032 (2020).
- [62] C.-K. Hu, J. Qiu, P. J. P. Souza, J. Yuan, Y. Zhou, L. Zhang, J. Chu, X. Pan, L. Hu, J. Li, Y. Xu, Y. Zhong, S. Liu, F. Yan, D. Tan, R. Bachelard, C. J. Villas-Boas, A. C. Santos, and D. Yu, Optimal charging of a superconducting quantum battery, *Quantum Sci. Technol.* **7**, 045018 (2022).
- [63] A. Galiautdinov, A. N. Korotkov, and J. M. Martinis, Resonator-zero-qubit architecture for superconducting qubits, *Phys. Rev. A* **85**, 042321 (2012).
- [64] Z. Ni, S. Li, L. Zhang, J. Chu, J. Niu, T. Yan, X. Deng, L. Hu, J. Li, Y. Zhong, S. Liu, F. Yan, Y. Xu, and D. Yu, Scalable Method for Eliminating Residual ZZ Interaction Between Superconducting Qubits, *Phys. Rev. Lett.* **129**, 040502 (2022).
- [65] A. C. Santos, Role of parasitic interactions and microwave crosstalk in dispersive control of two superconducting artificial atoms, *Phys. Rev. A* **107**, 012602 (2023).
- [66] M. Brekenfeld, D. Niemietz, J. D. Christesen, and G. Rempe, A quantum network node with crossed optical fibre cavities, *Nat. Phys.* **16**, 647 (2020).
- [67] L. Villa and G. D. Chiara, Cavity assisted measurements of heat and work in optical lattices, *Quantum* **2**, 42 (2018).
- [68] M. A. Norcia, M. N. Winchester, J. R. K. Cline, and J. K. Thompson, Superradiance on the millihertz linewidth strontium clock transition, *Sci. Adv.* **2**, e1601231 (2016).
- [69] E. A. Sete, A. Q. Chen, R. Manenti, S. Kulshreshtha, and S. Poletto, Floating Tunable Coupler for Scalable Quantum Computing Architectures, *Phys. Rev. Appl.* **15**, 064063 (2021).
- [70] Y. Yanay, J. Braumüller, T. P. Orlando, S. Gustavsson, C. Tahan, and W. D. Oliver, Mediated Interactions Beyond the Nearest Neighbor in an Array of Superconducting Qubits, *Phys. Rev. Appl.* **17**, 034060 (2022).
- [71] X. Mi, J. V. Cady, D. M. Zajac, P. W. Deelman, and J. R. Petta, Strong coupling of a single electron in silicon to a microwave photon, *Science* **355**, 156 (2017).
- [72] A. N. Cleland and M. R. Geller, Superconducting Qubit Storage and Entanglement with Nanomechanical Resonators, *Phys. Rev. Lett.* **93**, 070501 (2004).